Journal of South American Earth Sciences 69 (2016) 119–130

Contents lists available at ScienceDirect

Journal of South American Earth Sciences

journal homepage: www.elsevier.com/locate/jsames

Geochemical characterization in karst basin tributaries of the San Franciscan depression: The Corrente River, western Bahia, NE-Brazil

Karina L. Lecomte [a, b, *], Cristina C. Bicalho [b, c], Emmanoel V. Silva-Filho [b]

[a] Centro de Investigaciones en Ciencias de la Tierra (CICTERRA) CONICET/Universidad Nacional de Córdoba, Av. Vélez Sarsfield 1611, X5016CGA Córdoba, Argentina
[b] Departamento de Geoquímica, Instituto de Química, UFF, Niterói, RJ 24020-150, Brazil
[c] ICF Environnement, 30 rue Alexandre – Bât C, 92635 Gennevilliers, France

ARTICLE INFO

Article history:
Received 20 November 2015
Received in revised form
23 March 2016
Accepted 28 March 2016
Available online 30 March 2016

Keywords:
Karsts
Hydrochemical characterization
Seasonal behavior
Weathering
Trace and rare earth elements
Brazil

ABSTRACT

Karst aquifers are important freshwater resources for the growing population in Brazil. The sandstones of Urucuia plateau and the limestone of Bambui Group constitute important aquifer systems in the western part of Bahia state. The Corrente River provides ~30% of the total water flow of the São Francisco River and crosses karstified structures. Surface and groundwater samples were collected during the *dry period,* the *beginning of the wet season*, and the *wet season*. The main objective was to define sources and distribution of dissolved elements and to describe the geochemical processes that govern their mobility within the system. Water samples are classified into three groups, depending on the dominant weathering process. When carbonate dissolution governs, waters are bicarbonate–calcium-type; whereas when the atmospheric precipitation signal is present, the samples in siliciclastic terrain are more Cl^- - Na^+. Groundwaters reflect bicarbonate–mixed-type, with the highest dissolved concentrations. In contrast to the major elements, trace elements, including Rare Earth Elements (REE), show seasonal behavior: their concentrations increase with the *beginning of the wet season*, due to re-mobilization and release into the solution of adsorbed elements from the system and the atmospheric dust. The total dissolved REE concentration (800–7500 ng L^{-1}) is one order of magnitude more concentrated in karsts than in siliciclastic rocks. Principal component analysis was performed, explaining >77% of the variance. First factor extracted (REE, Y, Th, Al, Fe) explain the washout and enhancement of atmospheric dust weathering throughout the *beginning of the wet seasons*. The second component comprises variables related to karsts lithology, representing calcite and dolomite dissolution.

1. Introduction

Karsts are complex networks that include both surface and groundwater drainage. They are a geomorphologic and hydrogeological system formed by the dissolution of soluble rocks, such as limestone, dolomite and gypsum. Therefore, karsts are highly fissured carbonate rocks, with networks of fissures, caves, galleries, underground streams and natural wells (Kiraly, 2003). They also feed springs, which are, in turn, often used as sources of drinking water, or that give rise to wetlands that have high environmental value (Bradford and Watt, 1998). The evaluation of water geochemistry of representative springs and streams reveals important information about how karst aquifers function. In particular, geochemical signature as a product of water-rock interaction is an indicator of lithology (i.e., mineralogy) and the water residence time, which have been extensively investigated by geochemists (e.g., Chebotarev, 1955; Langmuir, 1997; Drever, 1997; Depetris et al., 2014). Furthermore, karst response to seasonal variation is other information that can be used to assess pollution risks and to determine groundwater management policies. A great deal of literature analyzes karst environments (e.g., Barbieri et al., 2005; Bonacci, 1987, 2004, 2015; Bonacci and Andric, 2008; Bonacci et al., 2012; Hartmann et al., 2013; Khaska et al., 2013; Mance et al., 2014; Ozyurt et al., 2014; Valero-Garcés et al., 2014). It is a well-known fact that water flowing in an unpolluted watershed acquires salt content principally from leaching of the host rock. However, the extent to which natural waters reproduce the

* Corresponding author. Centro de Investigaciones en Ciencias de la Tierra (CICTERRA) CONICET/Universidad Nacional de Córdoba, Av. Vélez Sarsfield 1611, X5016CGA Córdoba, Argentina.
E-mail address: karina.lecomte@unc.edu.ar (K.L. Lecomte).

http://dx.doi.org/10.1016/j.jsames.2016.03.011
0895-9811/

composition of the dissolving rocks depends on several factors, including both physical (temperature, residence time, flow rate, and water-rock ratio in the aquifer) and chemical (mineral susceptibility to weathering, precipitation of secondary minerals, presence of gas species). This paper reports new results for major, minor and trace elements in a karstic zone. This allows for the evaluation of the different sources, sinks, and fates of trace metals during water-rock interactions, and to identify the main chemical processes controlling the composition of their water discharges.

During recent decades, the state of Bahia has undergone a marked process of economic growth driven by agricultural modernization. This implied increased water consumption, along with an anthropogenic impact. Western Bahia is known for its abundant water resources (Gaspar, 2006). The karst aquifers in the San Franciscan depression are located downstream of the Urucuia sandstone aquifer, where the extraction of fresh water is intense. The Corrente River provides nearly 30% of the São Francisco River's water flow. Like most karst aquifers, the San Franciscan units are characterized by high contamination vulnerability, enhanced by short residence times and low self-depuration capability. Relatively to the behavior of contaminants in karst and porous aquifers, there is a considerable controversy about some concepts as contaminant, contamination, pollutant and pollution. According to Freeze and Cherry (1979) and Prohic (1989) every solute introduced into the hydrologic environment as a result of human's activities is referred to as a *contaminant*, regardless of whether or not the concentration reaches levels that cause significant degradation of water quality. The term *pollution* is reserved for situations where contaminant concentrations achieve levels that are considered to be objectionable. Particularly, karst aquifers present a very limited capacity of sorption and filtration which results in the rapid transport of contaminants. Moreover, due to high flow velocities and consequent short residence time, the decay process is less effective and contaminants can reach wells and springs very quickly. The present study region is even more vulnerable, due to its location, which is directly downstream a very erodible unit, the Urucuia plateau (CPRM/UFBA, 2007). While there has been some research on the geological and hydrological features in this region (e.g., Atman et al., 2011; de Sá C. Chaves et al., 2007; Galvão Carnier Fragoso et al., 2011 and references therein), few investigations have examined geochemistry.

This paper examines the factors controlling Corrente hydrological basin weathering and seasonal influence in order to characterize the chemical composition that results from the interaction between water—surface and grondwater—with siliciclastic and carbonate lithologies. It also analyzes the seasonal contrasting behavior between major and trace/rare earth elements. Trace elements and REE are important source tracers (Gaillardet et al., 2003). Knowing trace and RRE concentrations is important to determine baseline conditions and better understand climate and environmental changes, such as anthropogenic land use. The main aim of the present study is to contribute to a better understanding of the geochemical characteristics of a karst system, based on major, trace and rare earth element analysis of springs, streams and well samples. Their seasonal influence is interpreted through statistical analysis.

2. Materials and methods

2.1. Site description

The Corrente River, (42,732 km^2 catchment area and an average flow-rate of 36 m^3 s^{-1}), one of the most important tributaries of the San Francisco River, provides water to western Bahia (Fig. 1). With a tropical climate, the average annual rainfall in the basin during the last 74 years has been ~1000 mm. During the wet season—from October to April—the region receives 96% of its annual precipitation (HIGESA, 1995).

The geology of the Corrente basin is mainly characterized by the presence of two distinct lithologies: the sandstone plateau of the Urucuia Group and a series of carbonate formations. The predominant formation in the Corrente River basin is the Urucuia sandstones. These sandstones comprise a very large intracratonic basin, the San Franciscan basin, which extends N–S and is one of the most important granular aquifers in Brazil. The aquifer is composed by well-selected eolian quartz and feldspathic sandstones, with silicified intervals, and subordinated conglomerates. The rest of the basin is formed by carbonate and shale sequences interspersed with calcarenite, siltstone, dolomite and calcareous shales, mudstones and siltstones (e.g., Lima et al., 2007; de Sá C. Chaves et al., 2007; Galvão Carnier Fragoso, 2011; Simonetti and Fairchild, 2000). Finally, debris-ferruginous lateritic covers are predominant, while Cenozoic formations are restricted to small areas. Study area location and lithology are shown in Fig. 1. Fig. 1b) shows the entire Corrente hydrological basin with the uppermost catchments draining fully throughout Urucuia Gr. (in green).

Mainly due to the great hydrologic and other abundant natural resources this region underwent dramatic economic restructuring through modern agribusiness in the 1980s (Alves et al., 2011). This increased significantly the population of Western Bahia State, characterized by an important migration from Southern and Southeastern Brazil. The agribusiness in the study region has as main product the soybean, followed by corn, coffee and cotton, besides the cattle breeding. Those plantations have a common feature: they are mechanized, supported by center pivots irrigation (which has high water demand), and require high use of additives (NPK) and pesticides. Although agricultural activities have a great economic importance to the region, they trigger some alterations in the surrounding environment due to the disorganized and poorly planned occupation, like hydraulic regime alteration, natural vegetation suppression and an increase of soil erosion (Gaspar, 2006; Alves et al., 2011).

2.2. Sampling

High density polyethylene (HDPE) sample collection bottles were first double washed with sufficient amounts of distilled-deionized water (18 MΩ-cm), and then placed in a 10–20% (v/v) reagent grade nitric acid bath for three to five days. The sample bottles were then rinsed three times with distilled-deionized water, and doubled bagged in clean plastic bags. Surface and groundwater samples were collected during three sampling campaigns. In August 2011, the '*dry period*' sampling was conducted, while in November 2011 the "*beginning of the wet season*" sampling was carried out. Lastly, during March 2012, the "*wet season*" samples were collected. A total of 55 samples that correspond to 18 sampling points were collected and analyzed (Table 1, Fig. 1). The sampling points were chosen along the Corrente River network, from the Urucuia sandstone to the proximities of the Corrente River base level, before joining the main channel of the San Francisco River. The basin's headwaters are represented by surface water flowing through the Urucuia sandstone.

At each end-member (well, streams and springs), water was collected with a large, collapsible polyethylene container suitable that had been previously cleaned identically to the sample bottles. Streams samples were collected from bridges near of the river middle channel from 0.5 m below water surface. For the wells there were used 1.5 L bailers. All the wells were domestic or public wells used for water supply for local population and present depths ranging between 20 and 60 m. The collected water samples were

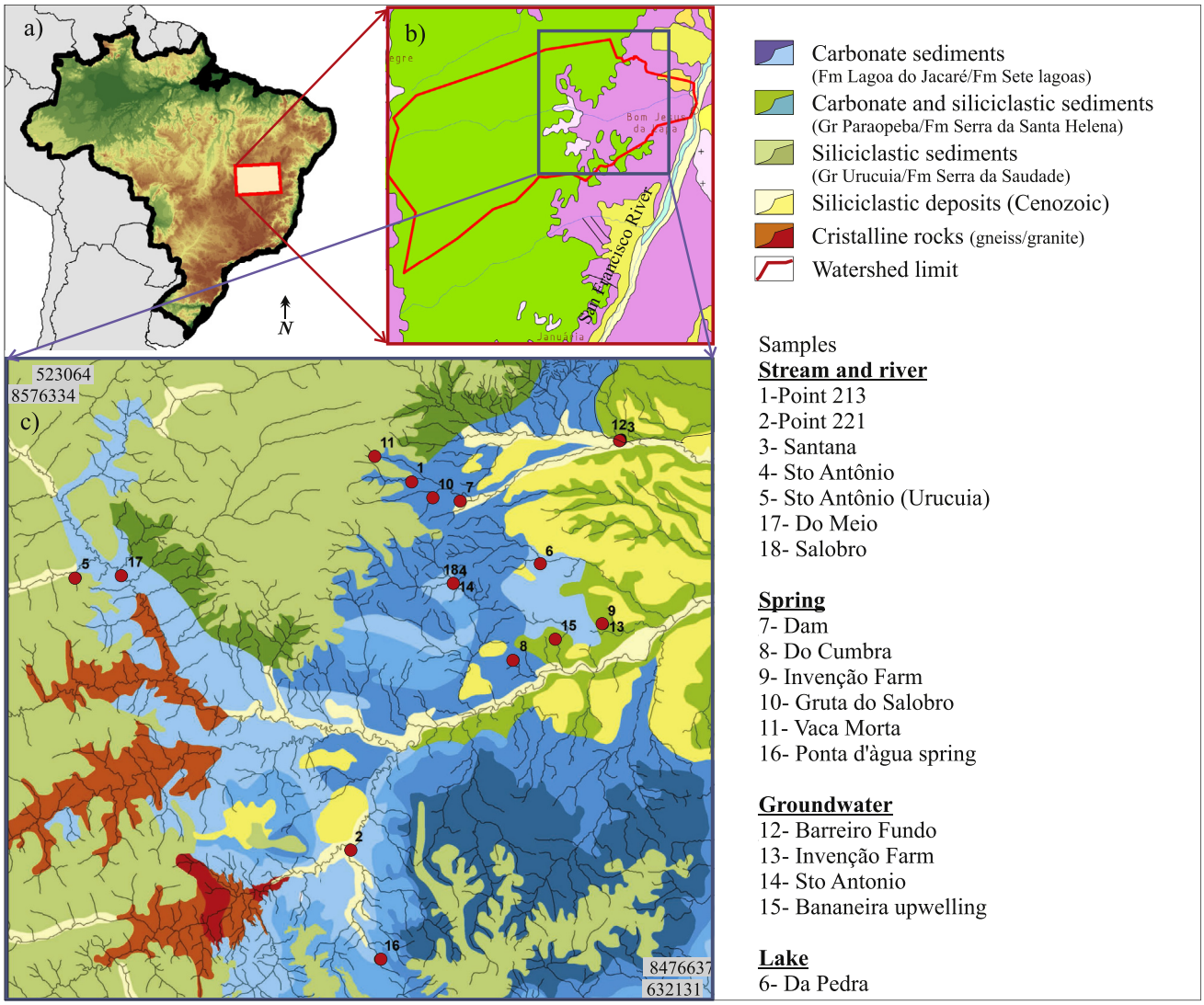

Fig. 1. a) Study area in Brazil, b) The Corrente River hydrological basin and c) outcropping lithology and sampling points locations of the lake, springs, streams and wells from the Corrente River Hydrological Basin.

Table 1
Date and sampling location of each sample.

Sample	Location name	Sampling date			UTMX	UTMY	Altitude (m)
		1- dry	*2- beginning of the wet season*	*3- wet*			
1	Point 213 stream	03/08/11	22/11/11	29/03/12	585,411	8,556,781	645
2	Point 221 stream	05/08/11	24–25/11/2011	30/03/12	576,039	8,500,242	460
3	Santana stream	03/08/11	22/11/11	28/03/12	617,441	8,563,006	469
4	Santo Antônio stream	02/08/11	24/11/11	31/03/12	591,866	8,541,043	554
5	Sto Antônio stream (Urucuia)	07/08/11		30/03/12	534,005	8,542,088	645
6	Lake Da Pedra	06/08/11	23–24/11/2011	28/03/12	605,006	8,544,033	496
7	Dam spring	03/08/11	22/11/11	29/03/12	592,907	8,553,791	598
8	Do Cumbra spring	04/08/11	23/11/11	28/03/12	601,060	8,529,523	481
9	Invenção Farm spring	06/08/11	23/11/11	28/03/12	614,543	8,534,900	452
10	Gruta do Salobro spring	02/08/11	22/11/11	29/03/12	588,681	8,554,253	643
11	Vaca Morta spring	03/08/11	24/11/11	29/03/12	579,783	8,560,651	696
12	Barreiro Fundo well	03/08/11	22/11/11	28/03/12	617,360	8,563,357	478
13	Invenção Farm well	06/08/11	23/11/11	28/03/12	614,661	8,534,859	452
14	Sto Antonio well	02/08/11	24/11/11	31/03/12	591,807	8,541,221	548
15	Ressurgencia da Bananeira well	04/08/11	23/11/11	28/03/12	607,368	8,532,641	459
16	Ponta d'àgua spring	05/08/11	25/11/11	30/03/12	580,490	8,483,647	555
17	Do Meio River	07/08/11	25/11/11	30/03/12	541,019	8,542,375	553
18	Salobro stream	02/08/11	24/11/11	31/03/12	591,834	8,541,202	552

then immediately filtered through 0.22 μm Millipore® cellulose acetate filters, rinsing the sample bottles three times before they were filled. The filtered samples for trace elements analysis were then immediately acidified to pH < 2 with ultra-pure nitric acid (65% Merck Millipore, sub-boiling, distilled in quartz). Samples for the major solutes were collected identically, except for the anion samples, which were not acidified. For each water sample, pH, temperature (°C) and electrical conductivity (EC) were measured *in situ* in separate sample aliquots, according to standard techniques. Alkalinity was titrated within a day using a digital titrator (HACH, Model 16,900).

2.3. Analytical determination, geochemical and statistical analysis

Major cations and anions (Table 2) were determined by ion chromatography on a Metrohm 850®, following standard methods (e.g., Welch et al., 1996). Anions were determined using a Metrossep A Supp 5–150 mm column, a self-regenerating anion suppressor, with Na_2CO_3 2.0 mmol/L and $NaHCO_3$ 1.0 mmol/L as eluent generator, and 18.2 MΩ cm^{-1} *water* as the reagent. The cations were measured with a Metrosep C4-100 mm column, with 1.7 mmol/L nitric acid (HNO_3) and 0.7 mmol/L dipicolinic acid (DPA) as eluent.

Trace element concentrations were determined using inductively coupled plasma - mass spectrometry (ICP-MS, Thermo Scientific® model XSeries 2) with a 5 point external calibration curve (prepared from SpecSol® tracked by NIST) using ^{115} an internal standard to account for matrix effects, differences in sample viscosity, solute build-up on the sampler and skimmer cones, and instrument drift during the analyses (Graham et al., 1996; Guo, 1996). In this study, 18 elements, including Li, B, Al, V, Cr, Mn, Co, Ni, Cu, Zn, As, Rb, Sr, Mo, Cd, Ba, Pb and U were measured. All elements were analyzed using the normal mode (argon gas) with CRI (collision reaction interface - helium gas) to avoid Ar interferences. The sensitivity of the ICP-MS was optimized for each analytical run, using a tuning solution containing 10 ppb (μg/L) of Li, Rh, Pb and U. Method detection limits (MDL) were calculated as three times the standard deviation of repeated 2% HNO_3 concentrations analyses in μg L^{-1}: 5×10^{-4} for Li, V, U and Co; 1×10^{-3} for Mn and Mo; 2×10^{-3} for Pb, Sr and Rb; 3×10^{-3} for Cu and Cd; 5×10^{-3} for Ni, 6×10^{-3} for Cr; 8×10^{-3} for As; 1×10^{-2} for Zn, 5×10^{-2} for Fe, 9×10^{-2} for Ba and 1×10^{-1} for Al. Blanks for the entire procedure ranged from 0.04 to 27% of the average sample values. The accuracy of the analytical protocol was ascertained based on repeated measurements of an externally certified reference solution (AccuTrace™ Reference Standard). The recoveries ranged from 92% for Cr to 106% for Ni. Regarding the analytical precision, the corresponding RSD values of all measured element concentrations in the reference material were less than 5%. For most of the analyzed stream waters, the charge imbalance between cations and anions was less than 5%, whereas all were less than 10%.

REEs were measured during distinct analytical sessions (Table 2) by direct measurement without pre-concentration (Smedley, 1991; Halicz et al., 1999) using a concentric nebulizer, with platinum sampler and skimmer cones. Isotopes ^{139}La, ^{140}Ce, ^{142}Ce, ^{141}Pr, ^{143}Nd, ^{146}Nd, ^{148}Sm, ^{149}Sm, ^{152}Sm, ^{151}Eu, ^{153}Eu, ^{157}Gd, ^{158}Gd, ^{159}Tb, ^{161}Dy, ^{163}Dy, ^{164}Dy, ^{165}Ho, ^{166}Er, ^{167}Er, ^{169}Tm, ^{172}Yb, ^{173}Yb, ^{174}Yb, and ^{175}Lu were monitored. In general, the elements were measured using the most abundant and least interfered isotopes. For the elements with more than one isotope measurement, the average concentration is below detection limits were generally in the low ng/L level for the REEs, and analytical precision, except for Eu, which was typically better than 8% RSD (relative standard deviation), and as high as 3% RSD for Ce. Despite of the use of collision reaction interface, analytical precision for Eu ranged from 3.9% RSD to as high as 32.9% RSD, with a mean (±standard deviation) of 18.8 ± 14.8% RSD. The accuracy of the method was tested using the National Research Canada SLRS-4 reference water standard and is in agreement with Yeghicheyan et al., 2001. Both Tables 2 and 3 present some elements with "n.d. (not determined)", there is data not available.

In order to evaluate and interpret minerals over or undersaturation, Saturation Index (SI) values were calculated through PHREEQC geochemical software (Parkhurst and Apello, 1999) in each sampling point. Moreover, to perform statistical analyses, physicochemical data were transformed into their logarithms whenever necessary to achieve univariate normality. These matrices were used as the basic input database. Regression matrix was performed to have a general idea of the relationship between elements and finally, a Varimax rotation factor analysis (Davis, 1986) was undertaken using the logarithmic database. This analysis combines numerous variables into some independent variables as principal components, which explain -in a statistically significant way-the largest amount of variation in the multivariate data.

3. Results and discussion

3.1. Hydrochemical characterization

The Corrente River hydrological basin has diluted waters with a mean value of total dissolved solids (TDS) of ~270 mg L^{-1} that reaches up to 700 mg L^{-1} in the groundwaters (Table 1). At the time of sampling, surface water temperature was quite constant, ranging between 20 °C during austral winter and ~28 °C during austral spring. On the other hand, groundwater and lake water temperatures were quite higher than those for surface waters streams, ranging between 26 and ~33 °C. There are no meaningful pH variations; waters generally have neutral pH, except Vaca Morta springs (sample 11), where pH values decreased until ~5.

Fig. 2 shows the seasonal TDS variation analysis. Generally, during the dry period, major dissolved concentrations increase, whereas concentrations are diminished during the *wet season*. This is a well-known process, which is caused by the combination of some factors: evaporation and groundwater influence provoke the increase of dissolved concentration during the dry period; and dilution by precipitation during *wet season*, which clearly reduces concentrations. Vaca Morta springs, along with Santo Antônio (Urucuia) stream and the Do Meio River (samples 11, 5 and 17, respectively), represent the most diluted samples. These are located in the northern sector of the study area and mainly drain siliciclastic sediments. Weathering kinetics of silicate minerals are much lower than carbonate dissolution, thus we expect to find lower chemical concentrations. On the other hand, the most concentrated samples correspond to those extracted from wells, due to longer residence time, which increases water-rock contact and facilitates rock weathering.

As expected in a karst-influenced region, cation dissolved concentration increased in the order $K^+ < Na^+ << Mg^{2+} < Ca^{2+}$. Na^+ behaves peculiarly: its concentrations are very low (mean = 5.7 mg L^{-1}, range = 0.2–45.8 mg L^{-1}) except in groundwaters showing higher Na^+ amounts (mean = 73.5 mg L^{-1}, range = 21–143 mg L^{-1}). These values are consistent with the higher dissolved solids concentration in groundwater and reflect Na-silicate weathering.

A Piper diagram (Piper, 1944) was performed (Fig. 3) to recognize different hydrochemical signatures. Most of the samples are clearly HCO_3^-- Ca^{2+} type. The exceptions are Vaca Morta spring (Sample 11) and Sto Antônio stream (Sample 5), which represent more chloride-sodic waters. The karst-type classification proposed by Bicalho et al. (2015) was not observed in the present Piper diagram (Karst 1, 2 and 3, Fig. 3). The main groups of hydrochemical

Table 2
Major physicochemical variables measured in each sampling period. The first number corresponds to the sampling period, 1: dry, 2: Beginning of the wet seasons, 3: wet. The second number corresponds to the sample number given in Table 1. nd: not determined.

Sample name		T°C	pH	CE	TDS	$HCO3^-$	Cl^-	$NO3^-$	SO_4^{2-}	Ca^{2+}	Mg^{2+}	Na^+	K^+
		°C		µs cm^{-1}	mg L^{-1}								
Point 213 stream	1-1	26.6	7.73	390	200	174.40	nd	nd	nd	nd	nd	2.48	2.31
	2-1	27.8	7.45	270	170	184.00	nd	nd	nd	48.00	3.10	1.96	2.28
	3-1	26.5	8.14	306	153	124.01	0.99	1.04	0.85	33.54	1.91	1.28	1.35
Point 221 stream	1-2	22.0	7.60	799	410	355.00	37.31	1.66	15.24	nd	nd	2.22	2.87
	2a-2	24.9	7.47	766	280	381.34	33.44	1.63	8.08	104.00	25.80	12.00	4.16
	2b-2	23.2	7.34	340	220	160.95	4.98	1.77	13.69	41.50	12.50	0.26	4.21
	3-2	25.0	7.86	654	326	338.48	14.78	2.36	7.70	87.30	23.50	8.77	3.15
Santana stream	1-3	25.0	7.80	600	300	258.20	16.89	0.69	14.57	nd	nd	23.06	3.58
	2-3	26.3	7.42	436	280	236.35	7.98	0.60	5.36	66.70	8.04	11.39	4.38
	3-3	27.1	8.06	508	254	253.38	12.14	1.22	12.59	71.80	10.20	15.45	4.05
Santo Antônio stream	1-4	22.0	7.61	605	310	283.00	8.10	1.29	12.50	nd	nd	7.92	2.11
	2-4	23.6	7.23	200	130	97.01	2.25	1.03	5.29	27.80	3.57	2.21	4.56
	3-4	25.2	7.93	599	299	320.24	6.05	2.12	10.13	102.00	9.73	5.45	2.34
Sto Antônio st. (Urucuia)	1-5	25.0	7.80	5.9	7.7	6.40	0.25	nd	nd	nd	nd	0.32	0.76
	2-5	28.3	6.36	–	5.5	3.50	0.58	nd	nd	0.14	0.01	0.42	0.70
Lake Da Pedra	1-6	26.5	8.60	258	120	93.80	5.69	nd	4.06	nd	nd	nd	nd
	2a-6	27.9	7.67	240	160	129.45	8.45	nd	8.71	nd	nd	5.14	9.85
	2b-6	26.0	6.54	150	100	nd	nd	nd	nd	26.90	6.16	5.23	11.10
	3-6	32.9	8.33	174	86	91.60	4.39	nd	2.72	18.70	3.89	3.13	7.36
Dam spring	1-7	26.0	7.20	358	180	161.00	2.30	nd	nd	nd	nd	5.80	2.95
	2-7	26.8	7.04	350	220	178.18	5.59	2.69	10.29	57.20	4.88	5.55	2.97
	3-7	26.5	7.69	428	214	162.55	3.32	3.92	6.55	73.32	11.00	4.54	1.82
Do Cumbra spring	1-8	24.2	7.21	503	250	364.00	nd	nd	nd	nd	nd	2.02	1.03
	2-8	24.5	6.91	310	200	158.82	1.52	6.40	2.74	58.60	2.14	0.92	0.60
	3-8	24.8	7.15	414	206	215.07	1.71	3.95	2.79	76.00	2.91	1.34	1.03
Invenção Farm spring	1-9	20.0	7.80	391	190	196.20	nd	nd	nd	nd	nd	0.65	1.01
	2-9	24.6	7.58	210	130	108.72	0.61	1.56	0.82	38.90	1.07	0.20	0.41
	3-9	24.8	7.63	225	112	108.68	0.83	5.02	0.88	40.60	1.21	0.44	0.86
Gruta do Salobro spring	1-10	26.8	7.58	540	390	253.40	4.60	nd	nd	nd	nd	5.85	2.27
	2-10	26.9	6.89	530	340	305.36	3.60	2.43	6.97	99.10	6.62	5.24	2.33
	3-10	26.7	7.33	615	307	316.20	6.45	3.74	12.47	103.00	8.21	7.03	1.99
Vaca Morta spring	1-11	21.2	5.40	17.3	nd	2.60	1.16	nd	nd	nd	nd	0.57	0.29
	2-11	23.3	4.64	20	4.6	2.15	2.26	nd	nd	0.22	0.01	0.93	0.83
	3-11	23.1	5.11	20	4	1.51	0.64	0.47	nd	0.13	0.01	0.80	0.40
Barreiro Fundo well	1-12	29.9	7.00	1145	590	160.00	64.63	nd	53.46	nd	nd	143.58	4.49
	2-12	29.0	6.66	1200	600	553.84	38.97	nd	16.64	108.00	25.60	100.20	3.41
	3-12	28.4	6.93	1145	572	540.12	54.30	2.31	61.57	112.00	26.30	119.66	3.58
Invenção Farm well	1-13	28.0	8.11	1400	700	324.80	251.63	nd	10.64	nd	nd	66.42	0.00
	2-13	26.1	7.59	830	530	373.27	78.92	nd	9.37	70.60	5.74	97.16	0.99
	3-13	27.6	7.89	716	367	344.20	44.15	nd	7.63	74.00	5.47	67.90	0.98
Sto Antonio well	1-14	26.1	7.04	905	470	362.40	28.23	29.96	26.46	nd	nd	22.38	7.01
	2-14	26.7	6.77	860	550	392.88	21.88	19.62	42.54	139.00	15.20	21.13	6.90
	3-14	26.8	7.22	993	497	408.93	23.84	26.54	20.09	147.00	16.00	23.03	6.78
Ressurgencia da Bananeira well	1-15	24.5	7.30	716	360	283.40	23.58	5.12	39.66	nd	nd	16.52	1.94
	2-15	25.1	7.39	570	360	342.05	8.31	3.19	14.12	90.80	10.70	45.78	15.36
	3-15	24.1	7.16	284	144	138.54	3.33	3.92	6.55	45.00	4.16	3.17	3.69
Ponta d'àgua spring	1-16	24.0	7.60	909	460	463.00	10.54	7.65	6.62	nd	nd	6.58	2.34
	2-16	23.0	6.56	220	140	114.89	3.50	1.23	1.37	21.60	9.88	2.21	7.60
	3-16	24.2	7.54	800	400	449.18	8.13	6.39	3.30	90.30	46.20	5.54	3.62
Do Meio River	1-17	25.0	8.30	41.5	10	21.20	nd	nd	nd	nd	nd	0.37	0.54
	2-17	26.1	6.65	40	30	25.03	0.89	nd	nd	6.27	0.39	0.48	0.59
	3-17	26.7	7.76	33	17	19.96	0.48	0.41	nd	6.28	0.31	0.52	0.37
Salobro stream	1-18	23.5	7.60	627	320	282.60	nd	nd	nd	nd	nd	13.51	2.22
	2-18	24.0	7.32	340	220	175.23	2.70	0.58	8.21	48.80	7.01	5.15	4.53
	3-18	26.2	7.93	700	350	250.55	5.40	0.81	13.08	66.50	6.43	7.95	2.92

water-types are: a) surface water draining siliciclastic rocks, b) surface water draining carbonate rocks, and c) groundwater. This grouping is also shown by the positive SI results, which are shown in Fig. 4. Dry period analysis is not included due to lack of data. Saturation Indexes (SI) are widely used to predict mineral precipitation in a solution with particular physic-chemical characteristics (e.g., Plumber et al., 1983; Charlton and Parkhurst, 2011; Nordstrom et al., 2015; Lecomte et al., 2016). If the solution is at equilibrium, the SI = 0. If the SI > 0, then the solution is supersaturated and the mineral would tend to precipitate; if the SI < 0, the solution is undersaturated and the mineral would tend to dissolve, if present (Nordstrom, 2003).

Three minerals show positive SI values in some samples: calcite, dolomite and aragonite (samples are ordered from > to < positive Calcite SI values). These minerals are carbonates, and samples with positive SI correspond to those that drain though karst formations (e.g., Samples 4, 3, 13, 2, 18, 16, 14), indicating that oversaturation and carbonate precipitation is possible. Moreover, the third sampling campaign (*wet season*) has a higher SI than the second campaign *(beginning of the wet season)*. Likewise, it is expected to find higher SI during the *dry season*, due to the major chemical concentrations.

Table 3
Trace and REE dissolved elements measured in each sampling period. The first number corresponds to the sampling period, 1: dry, 2: Beginning of the wet seasons, 3: wet. The second number corresponds to the sample number given in Table 1. nd: not determined. The subscript N denotes normalization.

Sample name	Al	Mn	Fe	Cu	Zn	As	Sr	Pb	Ba	Sc	Y	La	Ce	Pr	Nd	Sm	Eu	Gd	Tb	Dy	Ho	Er	Tm	Yb	Lu	Th	U	*LaN/LuN*
	$\mu g\ L^{-1}$																											
1–1	5.65	20.49	6.88	0.95	1.48	0.48	444	1.30	69.7	5.589	0.256	0.148	0.172	0.076	0.142	0.066	0.052	0.031	0.052	0.054	0.053	0.046	0.037	0.03	0.064	0.485	0.287	0.026
2–1	82.97	19.71	151.2	0.55	1.52	0.46	314	0.52	66.3	5.764	0.512	0.694	0.904	0.216	0.663	0.166	0.073	0.135	0.065	0.108	0.063	0.072	0.04	0.048	0.067	0.488	0.28	0.117
3–1	6.63	19.05	34.46	0.84	0.74	0.48	355	1.24	62.8	5.505	0.245	0.203	0.246	0.092	0.199	0.076	0.052	0.038	0.053	0.056	0.053	0.046	0.037	0.03	0.064	0.486	0.278	0.036
1–2	2.32	24.87	8.06	0.51	0.63	1.11	552	0.72	102.6	6.146	0.15	0.082	0.111	0.061	0.074	0.053	0.053	0.017	0.05	0.043	0.05	0.039	0.037	0.025	0.063	0.485	0.301	0.015
2a-2	59.52	24.03	91.73	1.36	1.80	1.23	541	1.66	86.6	5.312	0.379	0.313	0.462	0.122	0.317	0.106	0.062	0.069	0.057	0.078	0.057	0.058	0.039	0.038	0.065	0.486	0.313	0.055
2b-2	50.37	1.28	30.96	2.05	1.14	0.65	195	1.26	38.5	2.231	0.336	0.379	0.412	0.137	0.374	0.111	0.057	0.074	0.057	0.078	0.057	0.056	0.039	0.037	0.065	0.486	0.314	0.066
3–2	6.22	26.76	10.47	0.83	1.87	0.83	373	0.71	73.7	3.948	0.221	0.12	0.165	0.07	0.115	0.061	0.05	0.025	0.051	0.05	0.052	0.044	0.038	0.029	0.064	0.485	0.318	0.021
1–3	3.13	25.01	6.28	3.67	0.97	1.07	750	1.47	89.6	5.684	0.165	0.092	0.135	0.064	0.092	0.058	0.053	0.02	0.051	0.046	0.051	0.041	0.037	0.027	0.063	0.484	0.345	0.017
2–3	54.39	9.33	127.30	0.71	1.96	0.99	557	0.54	70.7	5.265	0.229	0.225	0.363	0.101	0.234	0.086	0.056	0.05	0.054	0.062	0.054	0.047	0.038	0.032	0.064	0.485	0.355	0.040
3–3	9.59	3.30	14.33	1.16	0.75	1.09	635	1.01	69.9	4.97	0.2	0.12	0.166	0.072	0.124	0.064	0.051	0.026	0.052	0.052	0.052	0.044	0.038	0.028	0.064	0.484	0.37	0.021
1–4	4.37	43.73	11.20	0.76	6.32	0.61	1024	0.80	61.1	4.428	0.121	0.073	0.113	0.059	0.066	0.052	0.047	0.013	0.05	0.04	0.05	0.037	0.037	0.023	0.063	0.484	0.337	0.013
2–4	548.40	4.35	362.00	1.75	1.25	0.40	205	0.54	47.8	2.64	1.11	1.195	1.561	0.42	1.474	0.342	0.112	0.286	0.09	0.239	0.089	0.145	0.05	0.106	0.075	0.508	0.281	0.181
3–4	3.99	40.65	5.26	0.56	1.80	0.56	875	0.36	69.1	4.129	0.25	0.118	0.152	0.071	0.119	0.062	0.052	0.027	0.052	0.053	0.053	0.046	0.038	0.03	0.064	0.484	0.345	0.021
1–5	8.35	0.82	13.37	nd	0.29	0.19	2	0.29	7.7	2.678	0.094	0.066	0.097	0.057	0.062	0.05	0.039	0.012	0.05	0.039	0.05	0.036	0.036	0.023	0.063	0.484	0.255	0.012
2–5	15.16	0.64	26.78	0.22	1.17	0.23	1	0.54	4.3	3.043	0.105	0.074	0.12	0.06	0.07	0.053	0.039	0.014	0.05	0.04	0.05	0.037	0.037	0.024	0.063	0.484	0.254	0.013
1–6	nd	nd	nd	nd	nd	nd	nd	nd	nd	nd	nd	nd	nd	nd	nd	nd	nd	nd	nd	nd	nd	nd	nd	nd	nd	nd	nd	–
2a-6	1170	7.39	719.80	1.79	1.37	0.59	143	1.56	15.0	2.642	0.61	0.737	0.994	0.239	0.765	0.205	0.072	0.16	0.071	0.15	0.071	0.095	0.044	0.073	0.071	0.539	0.265	0.118
2b-6	274.20	53.71	276.10	1.85	0.80	1.00	222	2.13	23.4	0.921	0.403	0.622	0.965	0.201	0.623	0.159	0.065	0.124	0.063	0.105	0.061	0.067	0.04	0.044	0.066	0.497	0.289	0.107
3–6	nd	nd	nd	nd	nd	nd	nd	nd	nd	nd	nd	nd	nd	nd	nd	nd	nd	nd	nd	nd	nd	nd	nd	nd	nd	nd	nd	–
1–7	4.45	1.72	4.37	0.09	0.43	0.34	479	0.35	79.7	5.364	0.099	0.072	0.105	0.058	0.061	0.051	0.05	0.012	0.05	0.038	0.05	0.036	0.037	0.022	0.063	0.484	0.281	0.013
2–7	7.00	1.00	8.83	0.85	1.25	0.35	451	1.26	73.7	5.41	0.116	0.085	0.115	0.061	0.078	0.053	0.049	0.014	0.05	0.04	0.05	0.036	0.036	0.023	0.063	0.484	0.286	0.015
3–7	3.06	1.04	6.48	3.31	2.88	0.41	554	4.29	76.2	5.557	0.122	0.084	0.107	0.06	0.072	0.053	0.05	0.014	0.05	0.041	0.05	0.037	0.037	0.023	0.063	0.485	0.301	0.015
1–8	2.40	12.61	1.71	0.09	0.20	0.46	577	0.31	14.4	2.086	0.107	0.068	0.096	0.057	0.061	0.05	0.04	0.011	0.049	0.038	0.049	0.036	0.036	0.022	0.063	0.484	0.284	0.012
2–8	13.32	4.21	6.82	0.66	0.63	0.33	327	0.53	8.8	0.771	0.124	0.106	0.138	0.066	0.096	0.056	0.041	0.02	0.051	0.042	0.05	0.038	0.037	0.024	0.063	0.484	0.263	0.019
3–8	5.19	20.70	2.97	0.59	1.17	0.35	445	0.36	15.2	1.439	0.119	0.085	0.121	0.061	0.077	0.053	0.041	0.014	0.05	0.041	0.05	0.037	0.037	0.024	0.063	0.484	0.277	0.015
1–9	2.72	126.9	5.44	1.24	0.59	0.63	295	1.06	14.7	0.349	0.093	0.063	0.101	0.056	0.057	0.05	0.04	0.01	0.049	0.037	0.049	0.035	0.036	0.022	0.063	0.484	0.287	0.011
2–9	13.48	1.42	8.37	2.03	0.75	0.26	139	3.34	2.8	nd	0.112	0.094	0.133	0.064	0.088	0.055	0.039	0.015	0.05	0.042	0.05	0.037	0.036	0.023	0.063	0.484	0.259	0.017
3–9	8.68	8.85	15.69	1.13	1.42	0.31	166	1.11	10.1	nd	0.115	0.096	0.147	0.064	0.092	0.057	0.04	0.017	0.05	0.042	0.05	0.037	0.036	0.024	0.063	0.484	0.26	0.017
1–10	1.87	7.56	3.24	1.86	0.75	0.27	683	0.70	79.4	3.869	0.186	0.159	0.128	0.074	0.127	0.061	0.051	0.022	0.051	0.046	0.051	0.041	0.037	0.026	0.063	0.483	0.318	0.029
2–10	5.90	11.21	7.30	0.61	0.57	0.27	668	1.26	83.4	3.887	0.358	0.409	0.233	0.126	0.338	0.093	0.058	0.053	0.055	0.065	0.055	0.053	0.039	0.033	0.064	0.484	0.314	0.072
3–10	1.31	10.75	4.44	1.36	1.23	0.31	732	2.54	84.4	4.003	0.345	0.428	0.16	0.128	0.337	0.092	0.057	0.048	0.055	0.062	0.055	0.05	0.038	0.031	0.064	0.484	0.33	0.076
1–11	25.92	0.66	254.70	0.05	0.78	0.26	3	0.42	24.6	3.346	0.214	0.682	0.624	0.248	0.767	0.162	0.065	0.102	0.06	0.079	0.056	0.052	0.038	0.034	0.064	0.484	0.255	0.121
2–11	221.40	1.69	110.00	0.65	2.22	0.28	4	1.16	36.5	3.073	0.423	1.714	1.49	0.584	2.002	0.364	0.109	0.264	0.078	0.15	0.067	0.078	0.041	0.05	0.066	0.485	0.255	0.294
3–11	14.46	0.63	85.15	2.75	5.49	0.25	2	4.03	14.3	0.349	0.165	0.444	0.387	0.179	0.505	0.121	0.054	0.067	0.055	0.064	0.053	0.045	0.037	0.028	0.063	0.484	0.254	0.080
1–12	282.20	266.9	1846.0	27.02	60.29	22.01	24,590	15.21	334.8	nd	0.88	0.575	0.343	0.538	0.508	0.471	0.383	0.065	0.479	0.354	0.482	0.338	0.353	0.208	0.617	4.832	2.532	0.011
2–12	nd	37.67	46.73	27.02	21.33	2.39	5741	40.65	145.5	nd	0.889	0.587	0.847	0.552	0.522	0.483	0.387	0.084	0.49	0.366	0.488	0.346	0.36	0.211	0.625	4.832	2.539	0.011
3–12	nd	28.20	84.06	11.09	13.28	2.23	5534	3.87	101.4	nd	0.87	0.575	0.866	0.548	0.507	0.473	0.389	0.089	0.488	0.362	0.49	0.346	0.361	0.217	0.626	4.832	2.546	0.010
1–13	nd	29.02	104.70	0.83	2.47	2.37	5711	4.39	119.1	nd	0.837	0.577	0.04	0.537	0.509	0.466	0.365	0.059	0.473	0.352	0.475	0.333	0.344	0.197	0.607	4.837	2.478	0.011
2–13	0.16	2.96	2.04	3.54	1.23	0.57	346	5.25	5.2	2.213	0.157	0.122	0.187	0.07	0.11	0.058	0.045	0.021	0.051	0.043	0.051	0.038	0.037	0.024	0.063	0.485	0.273	0.022
3–13	3.12	67.85	9.70	0.66	0.46	1.30	2043	1.43	27.3	1.912	0.141	0.078	0.128	0.059	0.067	0.051	0.041	0.013	0.049	0.04	0.05	0.037	0.036	0.024	0.063	0.484	0.282	0.014
1–14	1.75	1.04	5.65	1.79	0.99	0.72	1617	2.69	54.0	4.986	0.249	0.105	0.103	0.066	0.101	0.058	0.047	0.022	0.051	0.048	0.052	0.042	0.037	0.026	0.063	0.484	0.376	0.019
2–14	4.33	3.45	7.70	0.35	3.51	0.67	1607	0.38	51.5	5.259	0.255	0.121	0.121	0.07	0.113	0.061	0.048	0.024	0.052	0.05	0.052	0.043	0.037	0.028	0.063	0.484	0.376	0.022
3–14	nd	2.82	4.45	1.22	2.96	2.11	1600	3.74	52.6	nd	0.946	0.605	0.767	0.554	0.552	0.486	0.381	0.093	0.487	0.366	0.489	0.35	0.357	0.21	0.626	4.832	2.632	0.011
1–15	2.78	6.25	1.95	0.37	0.72	0.73	1235	0.29	62.0	4.378	0.178	0.116	0.122	0.067	0.105	0.059	0.048	0.02	0.051	0.045	0.051	0.04	0.037	0.025	0.063	0.484	0.35	0.021
2–15	77.72	4.46	65.58	2.73	2.35	0.60	905	3.23	64.7	3.426	0.326	0.3	0.453	0.12	0.31	0.102	0.057	0.061	0.056	0.072	0.056	0.052	0.039	0.035	0.064	0.484	0.327	0.053
3–15	230.00	2.75	156.90	1.53	2.59	0.34	304	0.79	33.7	1.433	0.534	0.59	0.659	0.205	0.638	0.169	0.069	0.117	0.064	0.116	0.064	0.076	0.042	0.054	0.067	0.5	0.273	0.100
1–16	5.52	5.74	5.01	0.26	0.64	0.50	268	0.34	86.1	3.571	0.212	0.133	0.149	0.073	0.131	0.064	0.052	0.025	0.052	0.051	0.052	0.043	0.037	0.027	0.064	0.484	0.344	0.024
2–16	166.10	2.24	160.90	1.44	0.73	0.54	81	0.39	36.2	1.24	0.578	0.655	0.679	0.228	0.75	0.19	0.072	0.138	0.067	0.125	0.066	0.082	0.042	0.055	0.068	0.493	0.265	0.109
3–16	6.07	16.69	4.59	0.90	4.23	0.49	236	0.30	73.5	2.89	0.303	0.166	0.187	0.084	0.175	0.074	0.053	0.034	0.053	0.059	0.055	0.05	0.038	0.033	0.065	0.484	0.322	0.029
1–17	11.26	4.10	20.92	0.03	0.72	0.20	27	0.30	27.2	2.93	0.111	0.086	0.137	0.062	0.084	0.055	0.043	0.016	0.049	0.041	0.05	0.037	0.037	0.024	0.063	0.483	0.256	0.015
2–17	66.00	5.35	186.80	0.60	1.46	0.24	24	1.06	26.0	2.373	0.312	0.227	0.41	0.103	0.264	0.091	0.052	0.053	0.056	0.072	0.057	0.055	0.039	0.04	0.065	0.486	0.255	0.040
3–17	24.88	1.21	107.70	0.03	0.22	0.22	23	0.34	24.8	2.489	0.149	0.103	0.155	0.067	0.102	0.06	0.043	0.021	0.051	0.047	0.051	0.041	0.037	0.027	0.064	0.484	0.256	0.018
1–18	4.91	20.03	8.97	0.47	5.99	0.67	1317	0.46	65.5	4.222	0.128	0.083	0.132	0.061	0.075	0.053	0.048	0.015	0.05	0.04	0.05	0.037	0.037	0.024	0.063	0.484	0.346	0.015
2–18	629.20	9.41	446.90	6.67	2.74	0.50	455	7.41	53.4	2.707	0.872	1.099	1.669	0.344	1.198	0.289	0.097	0.227	0.078	0.194	0.077	0.108	0.046	0.088	0.071	0.507	0.333	0.175
3–18	6.12	37.93	9.72	0.50	1.79	0.70	1279	0.56	76.6	4.471	0.137	0.077	0.118	0.059	0.07	0.052	0.048	0.014	0.05	0.041	0.05	0.038	0.037	0.024	0.063	0.486	0.361	0.014

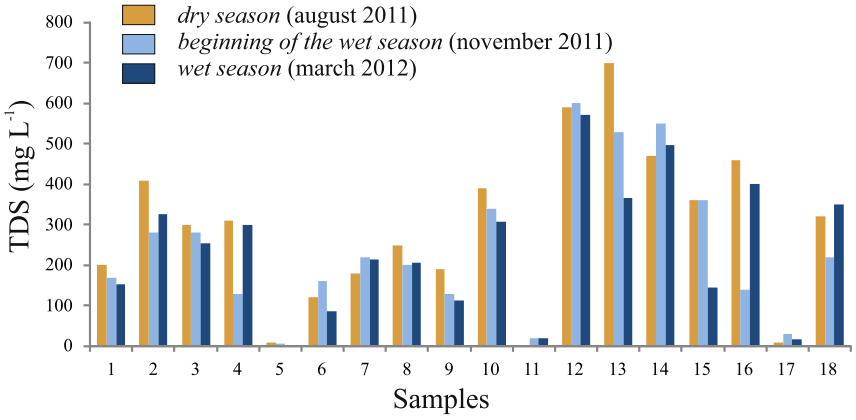

Fig. 2. Samples TDS values in each sampling period.

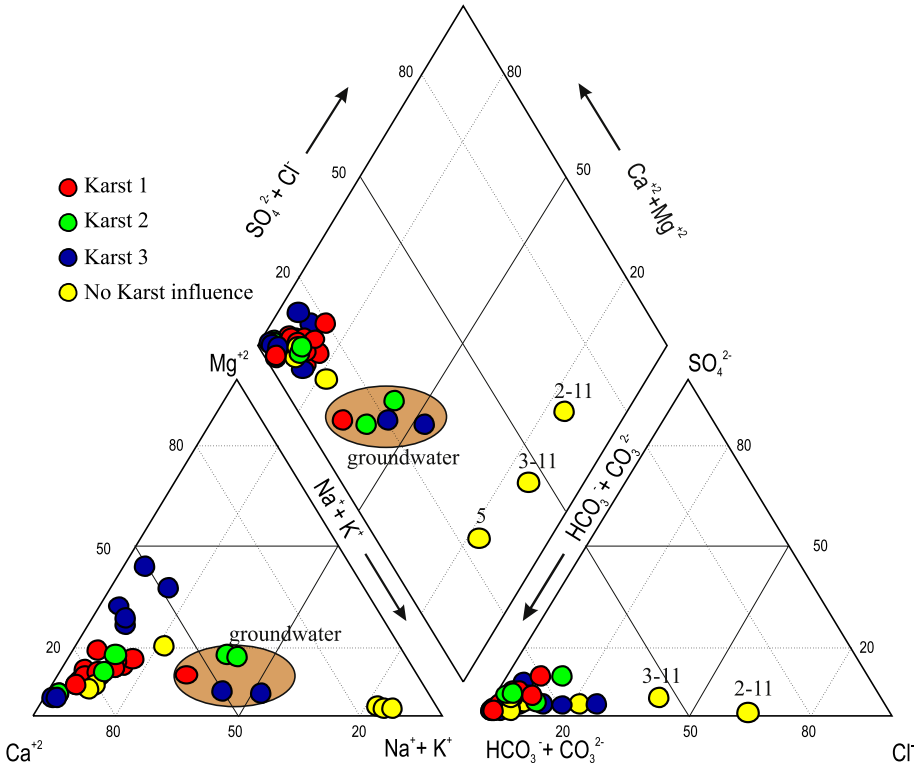

Fig. 3. Piper's (1944) diagram showing the major ion chemistry of sampled lake, rivers, streams, springs and wells. Karts 1, 2 and 3 are those karst-type classifications proposed by Bicalho et al. (2015).

3.2. Geochemical sources

Samples were plotted in scatter diagrams of anions and cations to analyze chemical weathering in the region. In the absence of halite, which is normally the case, Cl^- in water is mostly supplied by atmospheric precipitation in unpolluted areas. SO_4^{2-} is provided mainly by the dissolution of gypsum, which may be wind-transported or present in outcropping sediments. Scatter diagram representing halite mineral dissolution shows that, although Na^+–Cl^- regression coefficient is high ($r = 0.87$, not shown), Na^+ is more concentrated than the theoretical stoichiometric relationship (i.e., 1:1 M correspondence) in the mineral. A similar behavior occurs with gypsum, where Ca^{2+} is more concentrated than SO_4^{2-}. This suggests that dissolved chemistry in these surface waters is controlled by two general sources: atmospheric input and rock weathering. High bivariate relationships (Fig. 5a) between HCO_3^- and both Ca^{2+} and Mg^{2+} ($r = 0.90$ and 0.77, respectively) suggest carbonate weathering (calcite and dolomite). Calcite theoretical stoichiometric relationship is similar to relationship's slope, confirming it as a source. Although dolomite doesn't match with the theory, Mg^{2+} shows dependence with HCO_3^-. Moreover, dissolution of silicates (as anorthite) also results in HCO_3–Ca/Mg waters. Fig. 5a also shows groundwater samples (shown in red) and samples with low karst influence (in yellow).

To differentiate possible sources of dissolved elements (silicates vs carbonates), samples were plotted on the diagram represented in Fig. 5b, modified from Gaillardet et al. (1999). This diagram shows the end-members of silicate hydrolysis and carbonate or evaporite dissolution. The samples can be clearly seen on a line: one extreme is close to the ideal silicate source, while the other, along

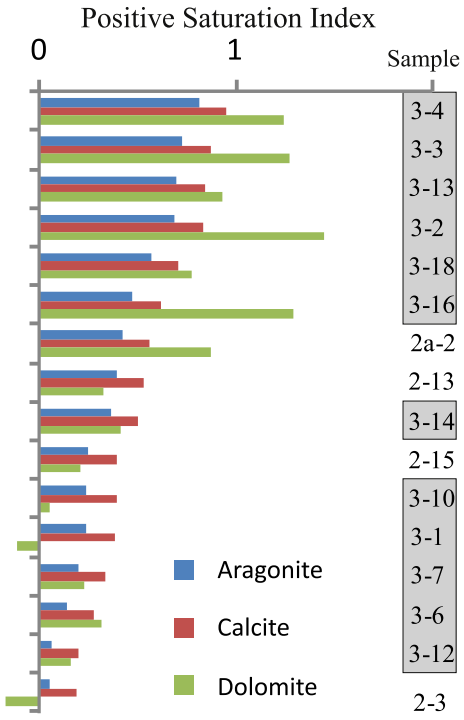

Fig. 4. Carbonate minerals saturation index (SI) along the Corrente River basin. Samples are ordered by calcite SI. *Wet season* samples are marked in grey.

with most of the samples, is above the carbonate end-member, revealing that ions are liberated into water by the weathering of such minerals. There are no differences among the sampling period. The higher amount of Na^+ (i.e., low HCO_3^-/Na^+ and Ca^{2+}/Na^+) revealing silicate weathering corresponding to Samples 5, 11, 12, 13, and 15 (Sto Antônio –Urucuia stream, Vaca Morta spring, Barreiro Fundo and Invenção Farm wells, and Ressurgencia da Bananeira well, respectively). The rest of the samples reflect that Na^+ comes from atmospheric precipitations. This is consistent with previous analyses: a) Samples 5 and 11 do not evidence karst as the dominant influence, b) groundwaters and resurgence evidence silicate weathering influence over carbonate dissolution. There is only one exception, found in Sample 14. This sample, a well in the karst formation, reflects both sources.

Finally, Fig. 5c shows a Gibbs (1970) diagram, where some of processes are highlighted: dilution, incongruent weathering, and evaporation, with an end-member of seawater and Amazonic signature. Most of the samples are plotted on the leftmost corner of the graph (Fig. 5c), suggesting that incongruent hydrolysis of silicate minerals, evaporation and dilution are not dominant processes. This emphasizes the idea that carbonate dissolution is the dominant process in these samples. However, silicate weathering is present in siliciclastic groundwaters and in samples with low carbonate influence. Some sampling legends were added.

3.3. Trace elements distribution

Table 3 lists the trace and rare earth elements (REE) measured in samples. Trace metal concentrations in the Corrente hydrological basin range from 0.3 to 40.6 μg L^{-1} for ultra-trace elements as Pb, and up to 1–24590 μg L^{-1} for minor elements (e.g., Fe and Sr). Groundwater samples have the most concentrated values (especially Barreiro Fundo wells, Sample 12), whereas those with no carbonate influence are the most trace diluted samples. This is consistent with major hydrochemical analyses based on kinetics

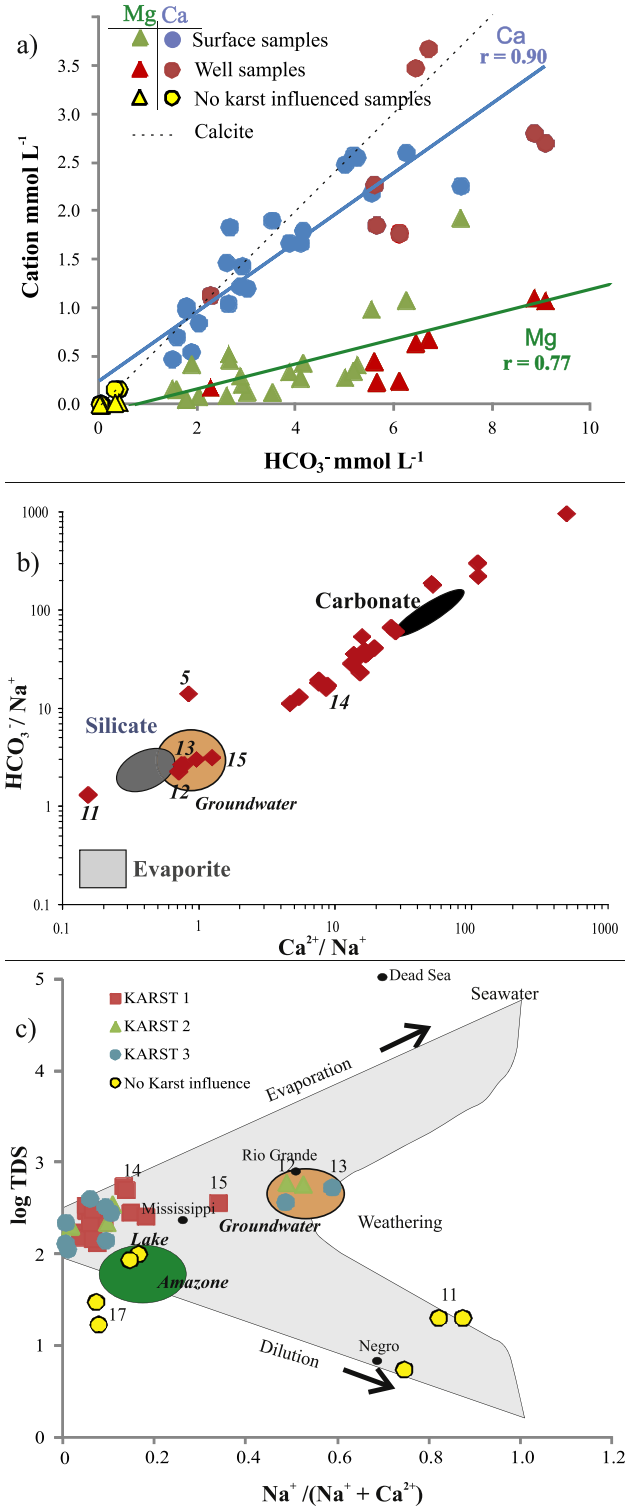

Fig. 5. a) Biplot relation between HCO_3^- and Ca, Mg. The surface, groundwater samples and those without karst influence are identified. b) Scatter graph showing likely solute sources in the studied system. Notice that plotted points mainly fall around carbonate composition. Some samples are labeled. c) Gibbs diagram (1970), showing processes which are likely to occur. Some samples are labeled. Note weathering processes in siliciclastic groundwater. Karts 1, 2 and 3 are those karst-type classifications proposed by Bicalho et al. (2015).

and residence time. The Da Pedra Lake has high concentrations of Al and Fe. The total sum of trace element concentrations in each

sample decreases in the order Sr > Fe > Al > Ba > Mn > Zn > Sc > Pb > Cu > As > Th > U > REE, with some slight differences between samples. Strontium and Ba have higher values than waters with no carbonate influence, due to their commonly replacement of Ca^{+2} or Mg^{+2} in calcite or dolomite structures, respectively (e.g., Bicalho et al., 2015).

Fig. 6a shows the range of dissolved trace elements normalized to upper continental crusts (UCC; McLennan, 2001) and the mean concentration of each sampling period. The water–rock ratios leads from 10^{-2} to 10^{-8} when normalized to UCC. Mobile elements that contain the highest normalized concentrations (i.e., ppm sample/ppm UCC > 10^{-4}) are Ca, Na, Mg, Sr, U, As, whereas K, Ba, Zn, Cu, Pb, Sc are present only in some samples (e.g., groundwaters). This relatively increased concentration is due the solubility of the minerals and their abundance in the outcropping rocks. Some of these elements (major cation, Sr, Ba) have high solubility, known as "large ion lithophile" or LIL elements (ionic potential <40 nm^{-1}). Depleted elements exhibit ppm sample/ppm UCC <10^{-6} at the Corrente River system, as Al and Fe. These elements are very insoluble, small and highly charged cations. All the remaining elements fall within the $10^{-6} - 10^{-4}$ concentration range.

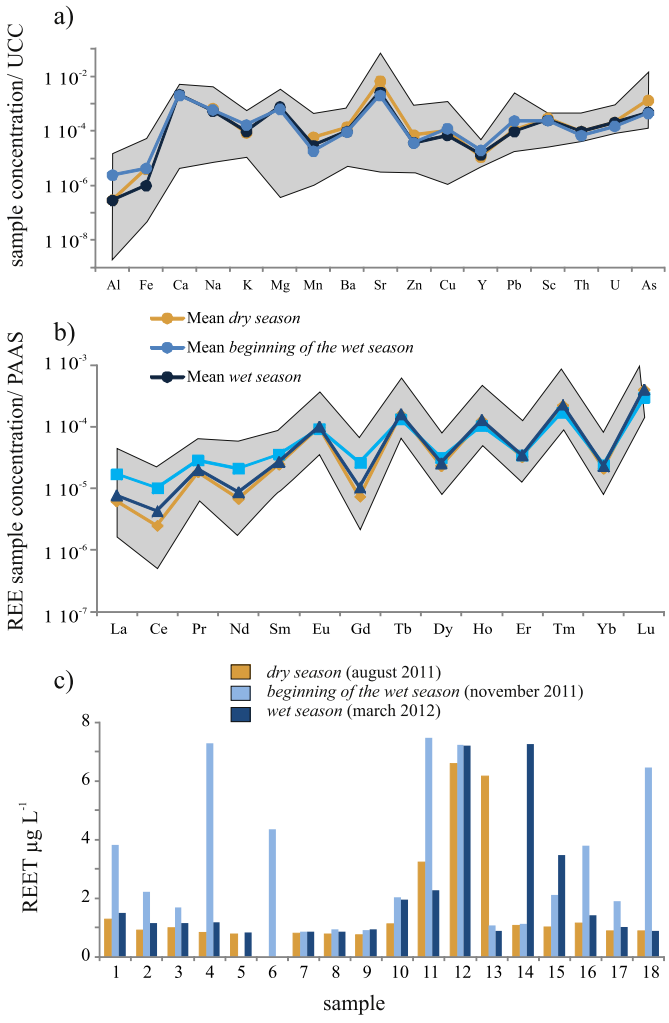

Fig. 6. a) and b) upper continental crust (UCC) normalized dissolved concentration and Post-Archean Australian shale (PAAS) normalized dissolved REE concentration distribution diagrams in the Corrente River surface and groundwater samples. The shadowed areas are determined by dissolved element variability; lines correspond to mean element concentration in the three sampling periods. There are also samples 1–5 and 1–12 in b) as examples. c) Seasonal dissolved REE distribution.

Analyzing the seasonal variation (Table 3), it is evident that many elements contain their highest values during the *beginning of the wet season*. Lecomte (2006) demonstrated that the first precipitation remobilized trace elements which had been trapped or adsorbed onto land surface sediments, releasing them into the solution.

Analyzing the total dissolved REE concentration in detail, it ranges from 800 to 7500 ng L^{-1}, with the highest concentrations present in Samples 11 and 4 (without karst influence) during the *beginning of the rainy season*, followed by groundwaters and that from the lake. Fig. 6b shows Post Archean Average Shales (PAAS)-normalized REE spidergrams (McLennan, 1989) and it is also represented the mean concentration of each period sampling. It is evident that behavior differs with respect to light (LREE: La to Nd) versus middle and heavy (MREE: Sm to Dy and HREE: Ho to Lu, respectively). There is a predominance of HREE and MREE over LREE, mostly in the groundwater samples (i.e., 12 and 14). This is also evidenced by the low La_N/Lu_N values, which range from 0.01 to 0.3 (Table 3), with the highest values during the *beginning of the wet season.* Another noteworthy point is the conspicuous positive Eu anomaly. This anomaly is widely used in petrology, due to its positive (enrichment) or negative (depletion) value, which results from the substitution of Sr by Eu in both feldspars (notably in Ca-plagioclase) and in carbonates (McLennan, 1989). In this case, the Eu anomaly is a direct consequence of calcite weathering. Likewise, the negative Ce anomaly occurs in response to the oxidation of Ce^{+3} to Ce^{+4} and its subsequent precipitation from solution as CeO_2 (Brookins, 1989).

Comparing REE dynamics with other environments, dissolved REE are more concentrated in the karst-influenced study area than in crystalline or volcanic terrains. Moreover, in the spidergrams obtained for samples collected in non-karstic landscape, the HREE normalized predominance is not evident. While most REE spidergrams from granite-dominated, volcanic sedimentary environments and estuaries sediments show a slight dominance of MREE over LREE and HREE (e.g., García et al., 2007; Hannigan and Sholkovitz, 2001; Lecomte, 2006; Lecomte et al., 2008; Pasquini et al., 2004; Rousseau et al., 2015, and references therein). A carbonate environment such as the Xijiang River (Xu and Han, 2009), is an example of PAAS-normalized REE patterns that have features in common with this work: positive Eu and negative Ce anomalies, and progressively HREE enrichment relative to MREE and LREE. The low REE dissolved concentration in the Xijiang River is mainly attributed to the interaction of high pH and low DOC concentration, whereas in the Corrente River there is no pH and REE relationship and DOC was not measured.

REE seasonal behavior is also shown in Fig. 6b, whereas Fig. 6c contains the REE concentration of each sample. Surface waters demonstrate a significant marked seasonal variation, with clearly increased concentration in the *beginning of the wet season*. This behavior can be explained by two mechanisms. The first one is the removal of adsorbed REE from sediments, as was previously stated for trace elements. The second process, atmospheric precipitation, represents a significant source of REE which probably comes from application of fertilizer (airborne soil particles, due to soil resuspension). The phosphate that composes the most fertilizers used in Brazil has magmatic source (carbonatites), which has high concentrations of REE (Abram, 2011). Concerning this hypothesis, an example of this is found in Samples 4, 18 (surface), and 14 (groundwater) collected in a restricted zone: surface waters exhibit up to six times more REE concentrated solution. García et al. (2007) showed a relatively high REE concentration in the atmospheric signature. Moreover, they found that once REE got into the surface, they were quickly removed by adsorption processes.

A regression matrix (not shown) evidences a statistically

relationship between REE and some elements. LREE has a demonstrable relationship, whereas most of MREE and HREE show a positive relationship with Y, Th, U, Cu, Zn, As, and Pb, evidencing their release into solution when the wet season starts. Moreover, REE are slightly related to the Cl^-, SO_4^{2-} and Na^+ concentration. It is known that the precipitations, which occur near the sea, present Na^+ and Cl^- high concentrations (e.g., Chang et al., 2005; Chudaeva et al., 2006; Jawad Al Obaidy and Joshi, 2006; Zhang et al., 2007a, 2007b; Zhao et al., 2008). In the region, air masses are issued from the south Atlantic, suggesting an atmospheric precipitation origin for those elements.

3.4. Statistical analysis

A principal component analysis was performed to obtain significant statistical relationship from the Corrente River dissolved elements. As a first approach, factor analysis (with Varimax rotation) was performed to convert a set of observations on possibly correlated variables into a set of values of linearly uncorrelated variables, called principal components. The result of this analysis indicated three principal components which explained >77% of the total sample variance. Factor loadings captured 51%, 19%, and 7% of the total variability, respectively. Table 4 shows factor loadings with their corresponding communalities. Communalities indicate the percentage explained by the factors. Most variables show communalities of >0.90, which points to the fact that most of the variability is accounted for by these factors.

The first factor (51.4% total variance) is interpreted as REE dominant influence (*PC-REE*), involving each rare earth element and also Y, Th, Al and Fe. To a lesser extent, Cu can be included with positive loading coefficients, indicating a direct relationship between them. Based on the information analyzed, it can be said that the *PC-REE* is interpreted as a group of elements from different sources including: a) by atmospheric input, b) by release to the solution via remobilization of Fe oxides and clays (aluminosilicate) which are adsorbed by REE, and c) by silicate weathering (e.g., biotite). When the wet season begins, the first precipitation causes the fine-grained sediments and clays that had been steadily adsorbing elements -mainly REE, Y, TH- change course and begin to release them into the solution. Afterwards a time, these elements are again removed from the dissolved phase into the solid phase. This adsorption process continues during *dry season* until the wet season starts again.

The second extracted factor (19.2% total variance) represents the control exerted by the carbonate lithology on the concentration of the main physicochemical variables (*PC-KARST*). The variables that have a significant loading in this factor are: TDS, EC, HCO_3^-, Ca, Sr, Ba, Mg, Cl, SO_4^{2-}, U and Na. In each variable, the coefficient has a

Table 4
Factor analysis results: Principal Component matrix with varimax rotation. Elements are ordered due to their statistical importance.

	Principal component			*Communalities*
	1 (51.4%)	2 (19.2%)	3 (7%)	
Dy	**0.988**	−0.116	0.013	*0.998*
Yb	**0.987**	−0.113	0.020	*0.994*
Er	**0.987**	−0.120	−0.002	*0.990*
Sm	**0.980**	−0.147	−0.014	*0.997*
Pr	**0.973**	−0.150	−0.058	*0.993*
Ho	**0.973**	−0.140	−0.001	*0.975*
Eu	**0.970**	−0.029	0.085	*0.976*
Y	**0.968**	0.048	−0.061	*0.975*
Tb	**0.967**	−0.165	−0.005	*0.978*
Gd	**0.966**	−0.093	0.002	*0.970*
Tm	**0.959**	−0.138	0.007	*0.959*
Nd	**0.956**	−0.110	−0.061	*0.972*
Ce	**0.947**	−0.141	0.136	*0.960*
Lu	**0.938**	−0.194	0.055	*0.933*
La	**0.937**	−0.101	−0.114	*0.962*
Th	**0.881**	−0.223	0.043	*0.949*
Al	**0.839**	−0.188	0.186	*0.922*
Fe	**0.833**	−0.107	0.352	*0.911*
T°C	−0.568	0.447	0.091	*0.943*
U	−0.111	**0.856**	0.271	*0.832*
Na	−0.026	**0.842**	0.118	*0.733*
TDS	−0.367	**0.834**	−0.170	*0.919*
Cl	−0.091	**0.820**	0.126	*0.908*
SO_4^{2-}	−0.042	**0.807**	−0.133	*0.805*
Ca	−0.466	**0.744**	−0.280	*0.931*
Sr	−0.378	**0.736**	−0.009	*0.952*
Sc	−0.214	**0.642**	0.426	*0.859*
Ba	0.064	**0.634**	0.363	*0.868*
K	0.499	0.548	0.176	*0.864*
NO_3^-	−0.408	0.183	**−0.763**	*0.865*
As	−0.022	0.450	**0.715**	*0.908*
pH	−0.270	0.122	**0.694**	*0.868*
Pb	0.172	0.123	0.041	*0.875*
Cu	0.528	−0.134	0.095	*0.951*
Mn	−0.045	0.206	0.215	*0.925*
Mg	−0.010	**0.612**	0.048	*0.949*
Zn	0.090	0.533	−0.032	*0.795*
	PC-REE	***PC-KARST***	***PC-land use***	
	**atmospheric signal*	**calcite/dolomite dissolution*	**land use*	
	**desorption process*	**cation exchange*	**acidification/As adsorption*	
	**silicate weatheing*			

positive loading, thus indicating that they have a direct relationship. In those areas where carbonate influence is present, *PCKARST*'s variables reach the highest concentration. Furthermore, the samples collected in the siliciclastic lithology show the lower concentrations in those variables. In this manner, the significance of carbonate and silicate lithology is evident, as well as seasonal influences on the production of solutes.

Finally, the third factor accounts for 7% of the total variance and underlines the significance of three variables: NO_3^-, As, and pH. In this case, coefficients have opposite loadings: NO_3^- has a negative loading, whereas As and pH have a positive coefficient, thus indicating that they have an inverse relationship. This points out that the third factor highlights samples with a high NO_3^- concentration and low As and pH values. The direct association that pH controls As adsorption processes is widely known. Nitrate concentration could be linked to changes in land use. Mudry et al. (2015) explain how land use changes result in a higher nitrate concentration, which, in turn, promotes CO_2 production (lowering pH). This relationship can explain the third factor: as a consequence of agriculture in the area, nitrate and dioxide carbon values increase, triggering the depletion of pH values and favoring As adsorption.

4. Conclusions

The Corrente River (42,732 km^2) with an average flow-rate of 36 $m^3\ s^{-1}$ and a significant influence of carbonate rocks, contains EC ranging between 4 and 1400 $\mu S\ cm^{-1}$ (mean EC ~500 $\mu S\ cm^{-1}$). Major physicochemical characteristics make water samples to be divided into three different groups: 1) Urucuia Group surface waters, type HCO_3^- - Cl^- have great variability through both the Ca^{+2} and Na^+— K^+ axes. They are evidence of silicate weathering, a clear atmospheric signal and no influence of carbonate rocks. 2) Wells, which are the most concentrated samples, due to their high water-rock contact time. Weathering processes are both silicate hydrolysis and carbonate dissolution with a mixing percentage dependent on surrounding lithology. Finally 3) is composed of carbonate draining surface samples. They are clearly HCO_3^- - Ca^{2+} water type, showing strong predominance of carbonate rocks as sources. Saturation index (SI), calculated by PHREEQC, show that this last group of samples is supersaturated in calcite, dolomite and aragonite; and that the SI is lower when the rainy season begins.

Seasonal analyses reveal that major and trace dissolved elements behave differently. While during precipitation events the concentrations of major elements are diluted, the concentration of trace and rare earth elements (REE) increases. This increase is due to both remobilization and desorption processes, as well atmospheric dust weathering.

REE concentrations in waters that drain from karstic terrains show a PAAS-normalized pattern, showing enrichment through high REE. Dissolved Lu concentration reaches 626 ng L^{-1} in karst groundwater, whereas it is depleted by one order of magnitude in non-carbonate surface waters. Finally, statistical analyses, namely matrix regression, and PCA, were used to classify variables into homogeneous groups. Principal component analysis shows that >50% of the variance is explained by REE, Y, Th, Al and Fe; with a statistically significant direct relationship ($p < 0.05$). This is interpreted as a silicate weathering process and also a desorption process which occurs during the *beginning of wet season*, with the first atmospheric precipitations. The second extracted factor explains 19% of the variability and comprises those variables related to karst lithologies (i.e., Ca^{2+}, HCO_3^-, Mg^{2+}, Sr, Ba, EC, TDS) and some variables associated as Na^+, Cl^-, U, SO_4^{2-}, Sc. These variables represent both, calcite and dolomite dissolution, as well as cation exchange occurring in karst environments. A third factor related to land use explains 7% of the total variability. Agriculture increases NO_3^- and CO_2 in solution, acidifying the environment. This is the first parameter that would indicate anthropogenic influences in the region.

In conclusion, during a hydrological year, the longer residence time in groundwater samples facilitates mineral weathering resulting in higher dissolved concentration. Moreover, in surface samples it is evident both controls: seasonal (dilution of major elements due to rainfall and enrichment of trace and rare earth elements) and a lithological control which clearly differentiate those samples taken from siliciclastic rocks from the carbonate ones. Geochemical variables allow for the identification of the sources of the dissolved elements. During the *beginning of the wet seasons* slightly acidic water drops weather atmosphere dust, and precipitation remobilizes trace and rare earth elements enriching their dissolved concentration in surface waters.

Acknowledgements

We acknowledge the financial support of the CAPES-MINCYT program (BR/red13/02). The field work and analysis were financed by CNPq (National Council of Technological and Scientific Development, of the Science and Technology Ministry of Brazil) and CPRM (Geological Survey of Brazil). K.L.L. is a member of CONICET, Carrera del Investigador Científico y Tecnológico (CICyT, Argentina). E.V. Silva-Filho is senior researcher at the National Council for Research and Development (CNPq, Brazil) and the Foundation for Research Support of Rio de Janeiro (FAPERJ). Language assistance by native English speaker Wendy Walker is gratefully acknowledged.

References

Abram, M.B., 2011. Os principais depósitos e ocorrências de fosfato no Brasil. In: Abram M.B., Bahiense I.C., Porto C.G., Brito R.S.C., (org). Projeto Fosfato Brasil — Parte 1, Geological Survey of Brazil (CPRM) Technical Report (Mineral Resources for Agriculture Series; 13), Salvador, pp 529.

Alves, R.R., Meira, S.A., Brasil, J., Feitosa, G.D.. Fragilidade Ambiental na Bacia Hidrográfica do Rio Preto - Oeste da Bahia. In: Mondardo M., (Org.) 2011. Espaços Agrários e Meio Ambiente: Bahia, Bahias. 1ed, Rio de Janeiro: Ponto da Cultura, pp 203.

Atman, D., Menegasse Velásquez, L.N., Fantinel, L.M., 2011. Controle estrutural na circulação e composição das águas no sistema aquífero cárstico-fissural do Grupo Bambuí, norte de Minas Gerais. Águas Subterrâneas 25 (1), 74–90.

Barbieri, M., Boschetti, T., Petitta, M., Tallini, M., 2005. Stable isotope (^2H, ^{18}O and $^{87}Sr/^{86}Sr$) and hydrochemistry monitoring for groundwater hydrodynamics analysis in a karst aquifer (Gran Sasso, Central Italy). Appl. Geochem. 20, 2063–2081.

Bicalho, C.C., Berbert-Born, M., Silva-Filho, E., 2015. Hydrogeological characterization of karst tributaries of the san Franciscan depression, river Corrente, west Bahia, Brazil. In: Andreo, B., et al. (Eds.), Hydrogeological and Environmental Investigations in Karst Systems, Environmental Earth Sciences, 1. Springer-Verlag Berlin Heidelberg. http://dx.doi.org/10.1007/978-3-642-17435-3_16.

Bonacci, O., 1987. Karst Hydrology with Special References to the Dinaric Karst. Springer, Berlin.

Bonacci, O., 2004. Poljes. In: Gunn, J. (Ed.), Encyclopedia of Caves and Karst Science. Fitzroy Dearborn, New York, pp. 599–600.

Bonacci, O., 2015. Karst hydrogeology/hydrology of dinaric chain and isles. Environ. Earth Sci. 74 (1), 37–55. http://dx.doi.org/10.1007/s12665-014-3677-8.

Bonacci, O., Andric, I., 2008. Sinking karst rivers hydrology: case of the Lika and Gacka (Croatia). Acta Carsologica 37 (2–3), 185–196.

Bonacci, O., Ljubenkov, I., Knezic, S., 2012. The water on a small karst island: the island of Korčula (Croatia) as an example. Environ. Earth Sci. 66 (5), 1345–1357.

Bradford, A., Watt, W.E., 1998. The role of groundwater in wetland protection: the Minesing Swamp, Ontario, Canada. In: Van Brahana, et al. (Eds.), Gambling with Groundwater, AIH XXVIII Conference, pp. 149–153.

Brookins, D.G., 1989. Aqueous geochemistry of rare earth elements. In: Lippin, B.R., McKay, G.A. (Eds.), Reviews in Mineralogy. Geochemistry and Mineralogy of Rare Earth Elements, 21, pp. 201–223.

Chang, C.T., Lin, T.C., Hsueh, M.L., 2005. Characterizinig precipitation chemistry in Changhua, Central Taiwan using weather conditions and multivariate analysis. Water, Air, Soil Pollut. 165, 61–75.

Charlton, S.R., Parkhurst, D.L., 2011. Modules based on the geochemical model PHREEQC for use in scripting and programming languages. Comput. Geosci. 37, 1653–1663.

Chebotarev II, 1955. Metamorphism of natural waters in the crust of weathering. Geochimica Cosmochimica Acta 8, 22–48, 137-170; 198-212.

Chudaeva, V.A., Urchenko, S.G., Chudaev, O.V., Sugimory, K., Matsuo, M., Kuno, A., 2006. Chemistry of rainwaters in the south Pacific area of Russia. J. Geochem. Explor. 88, 101–105.

CPRM/UFBA, 2007. Hidrogeologia da Bacia Sedimentar do Urucuia: bacias Hidrográficas dos Rios Arrojado e Formoso. In: Meta B, Caracterização Geológica e Geométrica dos Aquíferos – Revisão Geológica e Levantamento Geofísico (Comportamento das Bacias Sedimentares da Região Semi-Árida do Nordeste Brasileiro). CPRM/UFBA: Rede Cooperativa de Pesquisa, p. 72.

Davis, J.C., 1986. Statistics and Data Analysis in Geology, second ed. John Wiley & Sons, New York.

de Sá, C., Chaves, M.L., Benitez, L., Andrade, K Wanderson, Queiroga, G Nascimento, 2007. Estratigrafia e evolução geomorfológica do Grupo Bambuí na região de Morro Da Garça (MG). GEONOMOS 15 (2), 43–52.

Depetris, P.J., Pasquini, A.I., Lecomte, K.L., 2014. Weathering and the Riverine Denudation of Continents. Springer Science-Business Media B.V. Earth Sciences and Geography. http://dx.doi.org/10.1007/978-94-007-7717-0. Print ISBN: 978-94-007-7716-3, Online ISBN: 978-94-007-7717-0. Series Title: Springer Briefs in Earth System Sciences. 95pp.

Drever, J.I., 1997. The Geochemistry of Natural Waters. Surface and Groundwater Environment. Prentice Hall, New Jersey.

Fragoso, D Galvão Carnier, Uhlein, A., Sanglard, JC Destro, Suckau, G Labaki, Guerzoni, H Trópia Granja, Faria, P.H., 2011. Geologia dos Grupos Bambuí, Areado e Mata Da Corda na Folha Presidente Olegário (1:100.000), MG: registro deposicional do neoproterozóico ao neocretáceo da bacia do São Francisco. GEONOMOS 19 (1), 28–38.

Freeze, R.A., Cherry, J.A., 1979. Groundwater. Prentice Hall, p. 604 pp.

Gaillardet, J., Viers, J., Dupré, B., 2003. Trace elements in river waters. In: Drever, J.I. (Ed.), Surface and Ground Water, Weathering, and Soils. Elsevier, Amsterdam.

Gaillardet, J., Dupré, B., Louvat, P., Allègre, C.J., 1999. Global silicate weathering and CO_2 consumption rates deduced from the chemistry of large rivers. Chem. Geol. 159, 3–30.

García, M.G., Lecomte, K.L., Pasquini, A.I., Depetris, P.J., 2007. Sources of dissolved REE in mountainous streams draining granitic rocks, Sierras Pampeanas (Córdoba, Argentina). Geochimica Cosmochimica Acta 71, 5355–5368.

Gaspar, M.T.P., 2006. Sistema Aquífero Urucuia: Caracterização regional e propostas de gestão. PhD Thesis. Instituto de Geociências da Universidade de Brasília.

Gaspar, M.T.P., 2006. Sistema Aqüífero Urucuia: caracterização Regional e Propostas de Gestão. In: Instituto de Geociências. Universidade de Brasília, Brasília.

Gibbs, R.J., 1970. Mechanism controlling world water chemistry. Science 170, 1088–1090.

Graham, E.Y., Ramsey, L.A., Lyons, W.B., Welch, K.A., 1996. Determination of rare elements in Antarctica lakes and streams of varying ionic strength. In: Holland, G., Tanner, S.D. (Eds.), Plasma Source Mass Spectrometry. Developments and Applications. The Royal Society of Chemistry, London, pp. 253–262.

Guo, C., 1996. Determination of Fifty-six Elements in Three Distinct Types of Geological Materials by Inductively Coupled Plasma-mass Spectrometry (Unpublished M. S. thesis). University of Nevada, Las Vegas, p. 68.

Halicz, L., Galy, A., Belshaw, N.S., O'Nions, R.K., 1999. High-precision measurement of calcium isotopes in carbonates and related materials by multiples collector inductively coupled plasma mass spectrometry (MC-ICP-MS). J. Anal. Atom. Spectrom 14 (12), 1835–1838.

Hannigan, R.E., Sholkovitz, E.R., 2001. The development of middle rare earth element enrichments in freshwaters: weathering of phosphate minerals. Chem. Geol. 175, 495–508.

Hartmann, A., Barberá, J.A., Lange, J., Andreo, B., Weiler, M., 2013. Progress in the hydrologic simulation of time variant recharge areas of karst systems – exemplified at a karst spring in Southern Spain. Adv. Water Resour. 54, 149–160.

HIGESA, 1995. Plano Diretor de Recursos Hídricos - Bacia do Rio Corrente. Plano Setorial de Saneamento, Salvador.

Jawad Al Obaidy, A.H.M., Joshi, H., 2006. Chemical composition of rainwater in a tropical urban area of northern India. Atmos. Environ. 40, 6886–6891. http://dx.doi.org/10.1016/j.atmosenv.2005.01.031.

Khaska, M., Le Gal La Sallea, C., Lancelota, J., ASTER team, 2013. Origin of salinity in a coastal karst system: La Clape massif, SE France. Procedia Earth Planet. Sci. 7, 423–427.

Kiraly, L., 2003. Karstification and groundwater flow. Speleogenesis Evol. Karst Aquifers 1, 1–26.

Langmuir, D., 1997. Aqueous Environmental Geochemistry. Prentice Hall, New Jersey, p. 600.

Lecomte, K.L., 2006. Control Geomorfológico en la Geoquímica de los ríos de Montaña, Sierras Pampeanas, Provincia de Córdoba, Argentina. PHD Thesis. CIGeS. Facultad de Ciencias Exactas, Físicas y Naturales. Universidad Nacional de Córdoba, Argentina, p. 312.

Lecomte, K.L., Milana, J.P., Formica, S.M., Depetris, P.J., 2008. Hydrochemical appraisal of ice- and rock-glacier meltwater in the hyperarid Agua Negra drainage basin, Andes of Argentina. Hydrol. Process. 22 (13), 2180–2195.

Lecomte, K.L., Vignoni, P.A., Córdoba, F.E., Chaparro, M.A.E., Chaparro, M.A.E., Gargiulo, J.D., Kopalova, K., Lirio, J.M., Irurzun, M.A., Böhnel, H.N., 2016. Hydrological Systems from the Antarctic Peninsula under Climate Change: James Ross Archipelago as Study Case. Environ. Earth Sci. http://dx.doi.org/10.1007/s12665-016-5406-y.

Lima, O.N., Uhlein, A., de Britto, W., 2007. Estratigrafia do Grupo Bambuí na Serra da Saudade e geologia do depósito fosfático de Cedro do Abaeté, Minas Gerais. Rev. Bras. Geociências 37 (4), 204–215.

Mance, D., Hunjak, T., Lenac, D., Rubinić, J., Roller-Lutz, Z., 2014. Stable isotope analysis of the karst hydrological systems in the Bay of Kvarner (Croatia). Appl. Radiat. Isot. 90, 23–34.

McLennan, S.M., 1989. Rare earth elements and sedimentary rocks: influence of provenance and sedimentary processes. In: Lipin, B.R., McKay, G.A. (Eds.), Geochemistry and Mineralogy of Rare Earth Elements. Mineral. Soc. Am,Washington DC, pp. 169–196.

McLennan, S.M., 2001. Relationships between the trace element composition of sedimentary rocks and upper continental crust. Geochem. Geophys. Geosyst. 2. Paper Number 2000GC000109.

Nordstrom, D.K., 2003. Modeling low-temperature geochemical processes. In: Drever, J.I., Holland, H.D., Turkian, K.K. (Eds.), Surface and Ground Water, Weathering, and Soils, Treatise on Geochemistry, vol. 5. Elsevier- Pergamon, Oxford, pp. 37–65.

Nordstrom, D.K., Blowes, D.W., Ptacek, C.J., 2015. Hydrogeochemistry and microbiology of mine drainage: an update. Appl. Geochem. 57, 3–16.

Ozyurt, N.N., Lutz, H.O., Hunjak, T., Mance, D., Roller-Lutz, Z., 2014. Characterization of the Gacka River basin karst aquifer (Croatia): hydrochemistry, stable isotopes and tritium-based mean residence times. Sci. Total Environ. 487, 245–254.

Parkhurst, D.L., Apello, C.A., 1999. User's Guide to PHREEQC (Version 2) – A Computer Code Program for Speciation, Bath-reaction, One-Dimensional Transport and Inverse Geochemical Calculations. U. S. Geol. Surv. Water Resour. Investig. Rep. 99–4259.

Pasquini, A.I., Lecomte, K.L., Depetris, P.J., 2004. Geoquímica de ríos de montaña en las Sierras pampeanas: II. El río Los Reartes, Sierra de Comechingones, provincia de Córdoba, Argentina. Rev. la Asoc. Geol. Argent. 59 (1), 129–140. Argentina.

Piper, A.M., 1944. A graphic procedure in the geochemical interpretation of water analyses. Trans. — Am. Geophys. Union 25, 914–923.

Plumber, L.N., Parkhurst, D.L., Thorstenson, D.C., 1983. Development of reaction models for ground-water systems. Geochimica Cosmochimica Acta 47, 663–686.

Prohic, E., 1989. Pollution assessment in carbonate terranes - a review. In: LaMoreaux, P.E., Prohic, E., Zoetl, J., Tanner, J.M., Roche, B.N. (Eds.), Hydrologiy of Limestone Terranes, Annotated Bibliography of Carbonate Rocks, vol. 4, pp. 61–82. IAH, 10.

Rousseau, T.C.C., Sonke, J.E., Chmeleff, J., van Beek, P., Souhaut, M., Boaventura, G., Seyler, P., Jeandel, C., 2015. Rapid neodymium release to marine waters from lithogenic sediments in the Amazon estuary. Nat. Commun. 6, 7592. http://dx.doi.org/10.1038/ncomms8592.

Simonetti, C., Fairchild, T.R., 2000. Proterozoic microfossils from subsurface siliciclastic rocks of the Sao Francisco Craton, south-central Brazil. Precambrian Res. 103, 1–29.

Smedley, P.L., 1991. The geochemistry of rare earth elements in groundwater from the Carnmenellis area, southwest England. Geochim. Cosmochim. Acta 55, 2767–2779.

Valero-Garcés, B., Morellón, M., Moreno, A., Corella, J.P., Martín-Puertas, C., Barreiro, F., Pérez, A., Giralt, S., Mata-Campo, M.P., 2014. Lacustrine carbonates of Iberian karst lakes: sources, processes and depositional environments. Sediment. Geol. 299, 1–29.

Xu, Z., Han, G., 2009. Rare earth elements (REE) of dissolved and suspended loads in the Xijiang River, South China. Appl. Geochem. 24, 1803–1816.

Welch, K.A., Lyons, W.B., Graham, E., Neumann, K., Thomas, J.M., Mikesell, D., 1996. Determination of major element chemistry in terrestrial waters from Antarctica by ion chromatography. J. Chromatogr A739, 257–263.

Yeghicheyan, D., Carignan, J., Valladon, M., Bouhnik Le Coz, M., Le Cornec, F., Castrec-Rouelle, M., Robert, M., Aquilina, L., Aubry, E., Churlaud, C., Dia, A., Deberdt, S., Dupré, B., Freydier, R., Gruau, G., Hénin, O., de Kersabiec, A.-M., Macé, J., Marin, L., Morin, N., Petitjean, P., Serrat, E., 2001. A compilation of silicon and thirty one trace elements measured in the natural river water reference material SLRS-4 (NRC-CNRC). Geostand. Newsl.: J. Geostand. Geoanal 25, 465–474.

Zhang, M., Wang, S., Wu, F., Yuan, X., Zhang, Y., 2007a. Chemical compositions of wet precipitation and anthropogenic influences at a developing urban site in southeastern China. Atmos. Res. 84, 311–322.

Zhang, G.S., Zhang, J., Liu, S.M., 2007b. Chemical composition of atmospheric wet depositions from the yellow sea and east China sea. Atmos. Res. 85, 84–97.

Zhao, Z., Tian, L., Fischer, E., Li, Z., Jiao, K., 2008. Study of chemical composition of precipitation at an alpine site and a rural site in the Urumqi River Valley, Eastern Tien Shan, China. Atmos. Environ. 42, 8934–8942.